Novel procedure for generating continuous flash suppression: Seurat meets Mondrian

Oakyoon Cha
Department of Psychology, Vanderbilt University, Nashville, TN, USA
Graduate Program in Cognitive Science, Yonsei University, Seoul, Korea

Gaeun Son
Graduate Program in Cognitive Science, Yonsei University, Seoul, Korea

Sang Chul Chong
Graduate Program in Cognitive Science, Yonsei University, Seoul, Korea

David A. Tovar
School of Medicine, Vanderbilt University, Nashville, TN, USA

Randolph Blake
Department of Psychology, Vanderbilt University, Nashville, TN, USA

Continuous flash suppression (CFS) entails presentation of a stationary *target* to one eye and an animated sequence of arrays of geometric figures, the *mask*, to the other eye. The prototypical CFS sequence comprises different sized rectangles of various colors, dubbed *Mondrians*. Presented as a rapid, changing sequence to one eye, Mondrians or other similarly constructed textured arrays can abolish awareness of the target viewed by the other eye for many seconds at a time, producing target suppression durations much longer than those associated with conventional binocular rivalry. We have devised an animation technique that replaces meaningless Mondrian figures with recognizable visual objects and scenes as inducers of CFS, allowing explicit manipulation of the visual semantic content of those masks. By converting each image of these CFS sequences into successively presented objects or scenes each comprised of many small, circular patches of color, we create *pointillist* CFS sequences closely matched in terms of their spatio-temporal power spectra. Randomly rearranging the positions of the pointillist patches scrambles the images so they are no longer recognizable. CFS sequences comprising a stream of different objects produces more robust interocular suppression than do sequences comprising a stream of different scenes, even when the two categories of CFS are matched in root mean square contrast and spatial frequency content. Factors promoting these differences in CFS potency could range from low-level, image-based features to high-level factors including attention and recognizability. At the same time, object- and scene-based CFS sequences, when themselves suppressed from awareness, do not differ in their durations of suppression, implying that semantic content of those images comprising CFS sequences are not registered during suppression. The pointillist technique itself offers a potentially useful means for examining the impact of high-level image meaning on aspects of visual perception other than interocular suppression.

Overview

This paper introduces a novel visual animation technique for inducing continuous flash suppression (CFS), a very robust form of interocular suppression. This technique's novelty stems from its use of recognizable visual objects and scenes as the inducers of CFS. We start by describing our motive for developing this technique, then we describe how the interocular masks are created, and finally, we validate their utility in several psychophysical experiments.

Background and rationale

For decades, psychologists have deployed a variety of different psychophysical strategies for temporarily

Citation: Cha, O., Son, G., Chong, S. C., Tovar, D. A., & Blake, R. (2019). Novel procedure for generating continuous flash suppression: Seurat meets Mondrian. *Journal of Vision*, *19*(14):1, 1–22, https://doi.org/10.1167/19.14.1.

https://doi.org/10.1167/19.14.1 Received February 2, 2019; published December 2, 2019 ISSN 1534-7362

disrupting awareness of an ordinarily visible stimulus (Breitmeyer, 2015; Kim & Blake, 2005; Lin & He, 2009), with visual masking and binocular rivalry (BR) being chief among those strategies (see Hedger, Gray, Garner, & Adams, 2016, figure 1). And since its introduction by Fang and He (2005) and by Tsuchiya and Koch (2005), a variant of BR dubbed continuous flash suppression (CFS) has dominated in popularity owing to its remarkable potency. The essence of this effective dichoptic stimulation technique is the presentation of an ordinarily visible, static image to one eye pitted against an animated sequence of geometric figures or textures viewed by the other eye. In Tsuchiya and Koch's (2005) version of CFS, the figures were different sized rectangles of various colors, inspiring them to dub these images *Mondrians* after the 19th and 20th century Dutch painter Piet Mondrian whose abstract compositional style evolved to the use of the simplest of forms and colors devoid of figurative quality. The CFS technique quickly became popular, leading others to concoct a variety of derivative configurations for generating CFS including dense textures comprised of small, colored checks (e.g., Van Opstal, De Loof, Verguts, & Cleeremans, 2016), arrays of tiny ellipses differing in aspect ratio (Gray, Adams, Hedger, Newton, & Garner, 2013), band-pass filtered random noise (Han & Alais, 2018), and arrays of small grating patches intermingled with extended edges (e.g., Maruya, Watanabe, & Watanabe, 2008). When presented to an eye one after the other at a moderate frequency (e.g., 10 Hz), these arrays of geometric elements prove sufficient to suppress visibility of a static image viewed by the other eye for many seconds at a time, generating suppression lasting much longer than suppression durations associated with conventional BR (Ludwig, Sterzer, Kathmann, Franz, & Hesselmann, 2013).

Since coming on the scene, CFS has been a real workhorse in the study of visual processing outside of awareness (Gayet, Van der Stigchel, & Paffen, 2014; Lunghi, Lo Verde, & Alais, 2017; Moors, Hesselmann, Wagemans, & van Ee, 2017; Sterzer, Stein, Ludwig, Rothkirch, & Hesselmann, 2014; Yang, Brascamp, Kang, & Blake, 2014). The general strategy has been to present over test trials different kinds of static images (e.g., neutral vs. emotional faces) to one eye while the other eye views a potent Mondrian CFS sequence, the aim being to ascertain: (a) whether exemplars of those different stimulus types generate reliably different durations of suppression (e.g., Abir, Sklar, Dotsch, Todorov, & Hassin, 2018; Gray et al., 2013; Hung, Styles, & Hsieh, 2017; Jiang, Costello, & He, 2007; Moors, Boelens, van Overwalle, & Wagemans, 2016; Mudrik, Breska, Lamy, & Deouell, 2011; Rabagliati, Robertson, & Carmel, 2018; Stein, Sterzer, & Peelen, 2012; Rothkirch & Hesselmann, 2018; Yang, Zald, & Blake, 2007); (b) whether those stimuli, despite being suppressed from awareness, are capable of generating differential visual adaptation aftereffects (e.g., Kaunitz, Fracasso, & Melcher, 2011; Maruya et al., 2008; Stein & Sterzer, 2011; Sweeny, Grabowecky, & Suzuki, 2011) or exerting differential influences on perceived numerosity (Doi & Shinohara, 2016); (c) whether an object suppressed from awareness can nonetheless support accurate reach and grasp behavior (Ludwig et al., 2013; Roseboom & Arnold, 2011); (d) whether affectively tinted images draw spatial attention when those images are presented outside of awareness (Jiang, Costello, Fang, Huang, & He, 2006); (e) whether object priming or semantic priming can be induced by words or pictures suppressed from awareness (Peel, Sherman, Sperandio, Laycock, & Chouinard, 2019; Zabelina et al., 2013); (f) whether autonomic reactivity can be triggered by stimuli presented outside of awareness (Chiesa, Liuzza, Acciarino, & Aglioti, 2015); or (g) whether neural activity varies in magnitude or cortical distribution in response to different categories of stimuli presented during CFS (Almeida, Mahon, Nakayama, & Caramazza, 2008; Eo, Cha, Chong, & Kang, 2016; Fang & He, 2005; Kang, Blake, & Woodman, 2011; Lapate et al., 2016; Sakuraba, Sakai, Yamanaka, Yokosawa, & Hirayama, 2012; Sterzer, Haynes, & Rees, 2008).

In this paper we describe a complementary strategy for utilizing CFS as an inferential tool for investigating stimulus-specific concomitants of visual suppression of awareness. To date, CFS has been deployed to learn whether information processing within specific neural substrates survives perceptual suppression of the stimulus that triggers processing in those substrates. The emphasis, in other words, has been on the nature of the suppressed stimulus (e.g., animals vs. tools, upright faces vs. inverted faces, intact objects vs. scrambled images of those objects)—the CFS mask itself is purposely designed to be neutral with respect to specific figural attributes (e.g., consider the CFS toolbox created by Nuutinen, Mustonen, & Häkkinen, 2018). To put it in other words, random arrays of rectangles, ellipses or gratings do not imbue visual meaning to a CFS mask. To be sure, there are CFS studies that have attempted to identify low-level feature properties that empower a CFS display (Barrett, 2018; Han, Lunghi, & Alais, 2016; Yang & Blake, 2012), or have attempted to create CFS conditions that mitigate the impact of those properties (Ramamurthy & Blaser, 2018). To our knowledge, however, no one has explicitly manipulated the image content being depicted in a CFS display to create configurations that engender visual meaning in those images. The technique described in this paper was created with this aim in mind

and, moreover, to equate visually meaningful CFS stimuli and scrambled versions of those stimuli that are matched in terms of their low-level spatial frequency content, their root mean square (RMS) contrast, and chromatic diversity.

Inspiration for our work came from two earlier studies demonstrating that robust CFS could be induced by presenting to one eye a sequence of recognizable, natural scene images, all comprising outdoor environments and most including distinct objects characteristic of those environments (Blake, Goodman, Tomarken, & Kim, 2019; Kim, Kim, & Blake, 2017). As anticipated, those natural image sequences, just like Mondrian-based CFS, produced prolonged durations of invisibility of a contrast-modulated bull's-eye pattern viewed by the other eye. In a refinement and extension of that technique, we wanted to compare potency of CFS displays comprised of objects to CFS displays comprised of scenes. These two categories were chosen based on evidence purportedly showing that pictures of objects and pictures of scenes are processed by distinct neural mechanisms. Of course, scene pictures can include objects that are congruent with the scenic layout (e.g., a cow standing in a pastoral scene). Still, evidence suggests that scenic information and object information differentially activate regions within the occipital cortex, creating "gradients" of information about objects and spatial layout (Harel, Kravitz, & Baker, 2013; Kamps, Julian, Kubilius, Kanwisher, & Dilks, 2016; Kravitz, Peng, & Baker, 2011). To create the CFS animations necessary for our purposes, we selected object and scene images that have been used by others (see Methods), with the stipulation that scenes include only images portraying easily recognized spatial layouts containing few, if any, large, discrete objects in the scenes.

By way of preview, we discovered that CFS masks comprising different objects produced more robust interocular suppression than did CFS masks comprising different scenes. That finding did not surprise us particularly, for exemplars within those two image categories can differ notably in their global spatial configurations which, in turn, could impact their relative stimulus strength. What that finding did do, however, was prompt us to develop a novel technique that could equate those two categories of images in terms of spatial frequency and orientation, while preserving the specific connotations depicted by those two categories of images. That technique involved recreating each image as an array of small colored dots, mimicking the pointillist painting technique developed by 19th century post-impressionist French painter George Seurat (whose work predated that of Piet Mondrian by several decades).

Experiment 1: Comparison of CFS displays comprised of objects/scenes

Methods

Participants

Ten participants (five women and five men, mean age = 26.2 years) were recruited from Yonsei University. From the outset, our plan was to rely on recurrent Bayesian analyses to govern our sample size, knowing that the Bayes factor becomes progressively smaller with increasing sample size in cases where the null hypothesis becomes more and more likely than one's alternative hypothesis (Dienes, 2011; Rouder, 2014; Schönbrodt, Wagenmakers, Zehetleitner, & Perugini, 2017). This strategy resulted in a sample size of 10 participants, as the Bayesian analyses showed very strong evidence (Bayes factor >150) in favor of the hypothesis that the category of stimulus images comprising CFS sequences influences robustness of suppression.

All participants had normal or corrected-to-normal vision and good stereopsis, and they were naïve to the purpose of the experiment. Each provided written informed consent, and monetary compensation was provided for their participation. The study was approved by the Institutional Review Board of Yonsei University.

Apparatus

Stimuli were displayed on two gamma-corrected monitors (Sun Microsystems GDM-5410; resolution of 1280 × 960; frame refresh rate of 75 Hz) in a dark room. A two-mirror stereoscope reflected the images portrayed on the two monitors to the corresponding retinal locations of each eye. The participant's head position was stabilized by a head-and-chin rest, ensuring that the viewing distance of 65 cm was maintained. The luminance of the two monitors was linearized and equalized using customized gamma correction code (available at http://github.com/oakyoon/vcc-gamma). The equalized luminance of the two monitors was 84.4 cd/m^2 at maximum and the luminance of the gray background used through all experiments was 42.29 cd/m^2. All stimuli were generated using MATLAB (MathWorks, Natick, MA) and the Psychophysics Toolbox (Brainard, 1997; Pelli, 1997).

Stimuli and design

We selected images of single objects from the set described in Konkle, Brady, Alvarez, and Oliva (2010)

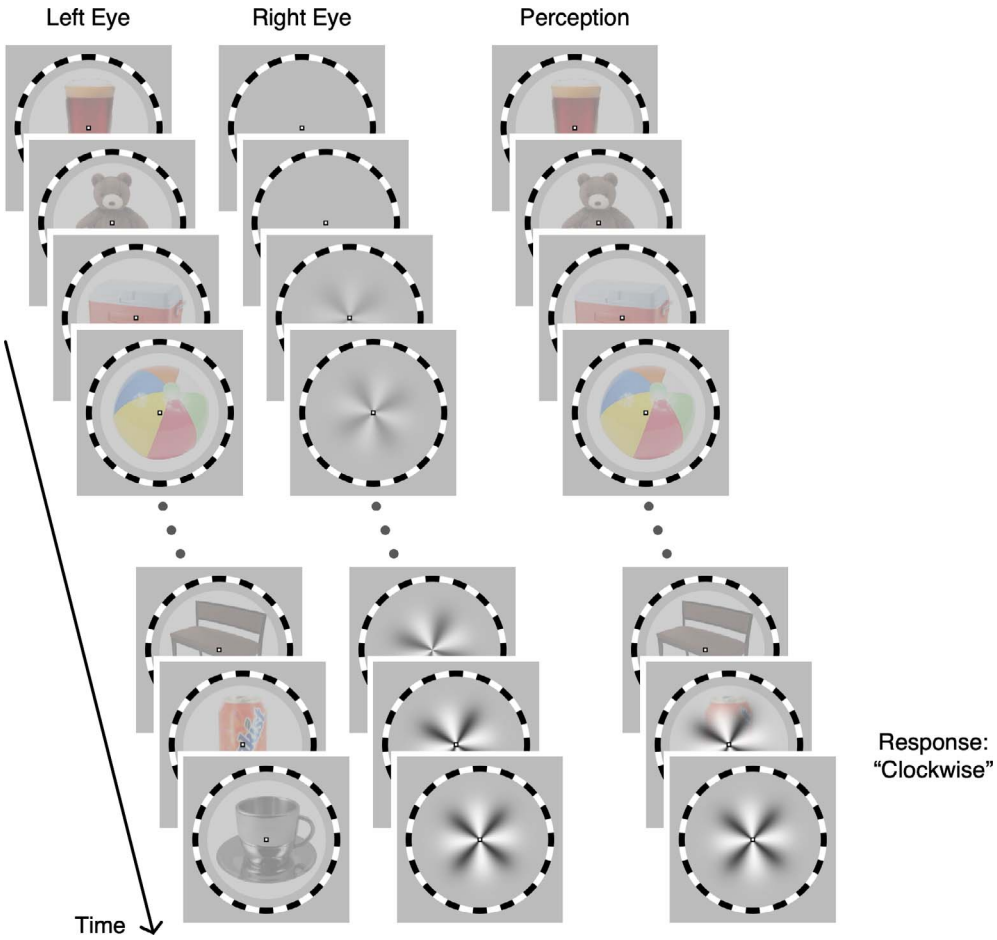

Figure 1. Procedures of Experiment 1. In each trial, different image sequences were presented to the left eye and to the right eye (i.e., to the separate video monitors). One eye viewed different exemplar images of objects (shown here) or of scenes, with successive images each being presented for 13.33 ms. The other eye viewed a rotating pinwheel grating whose contrast was initially low and then steadily increased over time, a maneuver ensuring that participants initially saw only the image sequence and not the pinwheel grating. Participants pressed one of two computer keys as soon as they could discern the grating's direction of rotation, which varied between CW and CCW randomly over trials.

and images of natural and urban scenes from the set described in Oliva and Torralba (2001). For our purpose, all images were sized such that each was centered within a circular window that comprised approximately 80% of the total image area occupied by each CFS mask display (see Figure 1). From the set of object images, we discarded those in which the object occupied more than 60% or less than 20% of that area, to ensure that object images were not cropped by the circular window while being large enough to be recognizable. For each image from both data sets, we calculated the average luminance, RMS contrast, and spectral power distributions of grayscale-transformed versions of those images. Images defined as outliers by a criterion amount established by a standard shoulder method were discarded from the final image set, resulting in retention of 503 object images and 720 scene images, which, in the actual experiment, were rendered in color. RMS contrast values of the retained object images ranged from 17% to 39% and RMS contrast values of the retained scene images ranged from 17% to 26%. In both of those image sets, individual RMS values were uniformly distributed within those ranges. Among the object images were many that are graspable (e.g., a cup) but also many that are not (e.g., a car). Among the final set of scene images were ones portraying natural environments (e.g., seashore) and others portraying urban environments (e.g., buildings). All 1,223 images were resized to 200 × 200 pixels (4.40° × 4.40°) and windowed by a circular aperture 200 pixels in diameter. These images were presented with 14% opacity on a uniform gray background. That value was selected based on pilot work aimed at creating CFS masks that would permit the target stimulus viewed by the other eye to achieve dominance on most of the test trials, each of which lasted 15 s.

To create object-based and scene-based CFS masks, we created animations of images drawn randomly from one category and presented in succession at a rate of 9.375 Hz (8 video frames/image, where a video frame was 13.33 ms), a value close to the modal display rate used in conventional CFS displays. A given CFS mask could be presented on either the left-hand or the right-hand video monitor. The monocular target stimulus pitted against the CFS mask was a circular-shaped pinwheel figure consisting of eight alternating black and white sectors whose luminance profile was defined by a sinusoidal function and circular border by a logistic function to eliminate sharp edges. The pinwheel target initially appeared at a very low contrast 600 ms after the CFS sequence started, and its contrast then smoothly increased to 100% over 9.4 s and stayed at 100% until the trial ended. During the period of increasing contrast, the target's contrast C varied according to the following formula: $C(t) = \log_{10}(1 + 9 \times (t - 0.6) \div 9.4)$. On any given presentation, the pinwheel's sectors rotated either clockwise or counter-clockwise at 4 rpm. Both the CFS mask and the pinwheel target were centered within ring-shaped fusion frames (inner diameter: 5.29°, thickness: 0.22°), with a central fixation point (a white square framed by black lines extending 0.18° × 0.18°) located at the centers of left- and right-eye displays (see Figure 1 for a schematic of these displays).

In Experiment 1, the aim was to determine target breakthrough times (BTs) for each category of CFS mask (object and scene). Over trials, the eye receiving the CFS mask and the eye receiving the target were counterbalanced over an irregular sequence. With 24 trials of repetition, the experiment consisted of 96 trials (object/scene × left eye/right eye × 24).

Procedures

Each trial began with presentation of the fusion stimuli and fixation point. This signaled the participant to fixate the central fixation point and press the spacebar on the computer keyboard to initiate a trial, an example sequence of which is illustrated in Figure 1. In this experiment, the CFS mask appeared abruptly followed 600 ms later by the gradual presentation of the rotating pinwheel target, achieved by ramping the target's log-contrast from 0% to 100% over the initial 9.4 s, after which it remained unchanged until the participant made a response indicating the direction of rotation of the pinwheel (clockwise or counter-clockwise). Because of the brief delay between the initial, abrupt onset of the CFS mask and gradual appearance at the low contrast pinwheel, participants always perceived the CFS mask exclusively at the beginning of each trial. Eventually the direction of rotation of the pinwheel target became sufficiently conspicuous for the participant to report its direction of rotation, which was done by pressing one of two keys promptly and accurately. Trials were terminated if the participant failed to make a response within 15 s. Before formal data collection, a practice session ensured that participants were familiar with the stimuli and that they understand the task.

Analysis

JASP statistics software (JASP Team, 2018) was used to conduct Bayesian analyses. Before analyzing BTs, we rejected the trials on which a participant reported the incorrect direction of rotation of the target stimulus (M: 0.95%, SD: 2.65%) or did not report seeing the target (M: 2.19%, SD: 3.94%). To compensate for individual differences in BTs (cf. Blake, Goodman,Tomarken, & Kim, 2019), we normalized each person's data by computing the grand mean BT for each person, and then divided each of that person's individual BTs by that grand mean.

Results and discussion

The scatterplot in Figure 2a summarizes the mean BT for object-based CFS and scene-based CFS for each of the 10 individuals. It is immediately obvious that object-based CFS masks produce longer BTs than do scene-based masks, as evidenced by the consistent appearance of data points below the diagonal of the scatterplot. Also, as expected based on earlier work (e.g., Gayet & Stein, 2017), we see that BTs vary substantially among individuals.

Figure 2b shows the normalized BTs averaged over the 10 observers for each of the two categories of CFS mask. Those averages just reiterate the difference in CFS robustness evidenced by the scatterplot in Figure 2a. An even more complete picture of those differences is revealed by the shift-plot format (Rousselet, Pernet, & Wilcox, 2017) in Figure 2c, in which BTs measured on every single trial of the experiment and normalized over participants are plotted separately for the two conditions (object trials in red, scene trials in yellow). Bayesian t tests confirm the obvious: normalized BTs for CFS mask comprised of objects are larger than 1 ($M = 1.248$, $SD = 0.045$, $BF_{10} = 350{,}197$), and normalized BTs for CFS mask comprised of scenes are smaller than 1 ($M = 0.764$, $SD = 0.037$, $BF_{10} = 1.021 \times 10^6$, note that these statistical results are interdependent). In other words, object-based CFS masks create more robust interocular suppression (i.e., longer BTs) than do scene-based CFS masks.

It is possible, of course, that the difference in CFS potency between objects and scenes has nothing to do with recognition of the content of those streams of

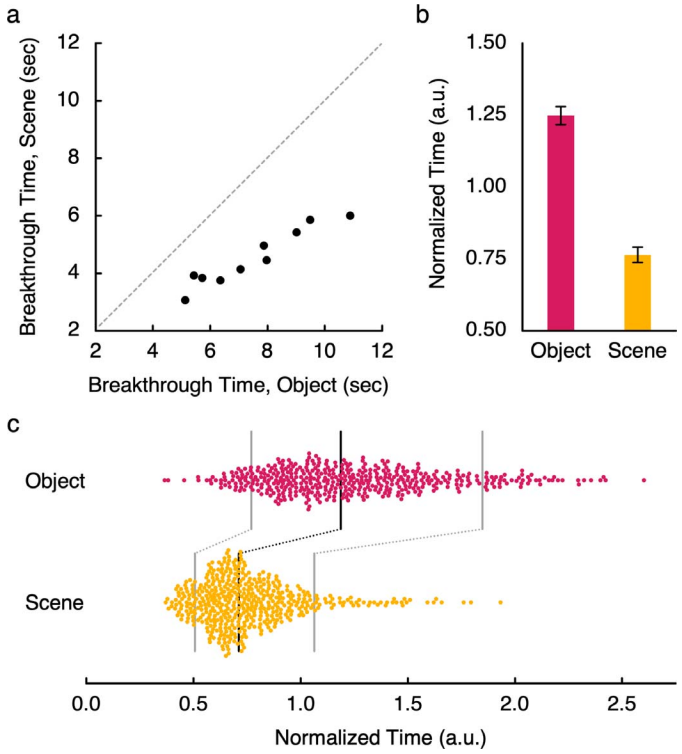

Figure 2. Results of Experiment 1. (a) Each dot plots the average breakthrough time (BT) for a participant measured for the object sequence trials and for the scene sequence trials. (b) The bar chart shows normalized BTs for object and for scene sequences averaged over all participants; error bars indicate 95% confidence intervals. (c) Using the shift-plot format (Rousselet et al., 2017), these clusters of data points show normalized BTs for every individual trial aggregated over all participants, for object and for scene sequences. Each dot designates the BT for a given trial, black lines indicate 50th percentile, and gray lines indicate 10th and 90th percentiles.

images but instead, is attributable to differences in the spatio-temporal energy produced by those CFS sequences. This idea can be formalized in several different ways. One way is to use dissimilarity matrices that specify the average difference in RGB values of all pixels in all possible pairs of images (Figure 3). Color is used to signify the magnitude of those differences, using the coding scheme described in the figure caption. Obviously, object images are more similar to one another than are scene images, and one likely reason for that is that the backgrounds are more uniform across object images. With this in hand, consider the temporal energy created by a CFS mask comprising a sequence of two successive images drawn from the same image category, conditions actually tested in Experiment 1. The mean of the change in luminance created when a given object image is replaced by another object image is very likely to be less than is the mean of the change in luminance created when given scene image is replaced by another scene image. This is going to be true over all successive image changes comprising the CFS sequence, meaning that the amplitude of the temporal frequency energy associated with object-based CFS masks will be less than the energy associated with scene-based CFS masks.

The same picture emerges when considering the spatial frequency content of object images and scene images used in Experiment 1, as summarized by the spectra in Figure 4. The plot on the left shows that object images tend to have more energy, on average, than do scene images. At least part of this difference is attributable to the object images having higher RMS contrasts, on average, than did scene images. The plot on the right shows that within our sample of images, scenes varied more in amplitude over all spatial frequencies than did object images. This latter difference is a reflection of the weaker similarity RGB luminance values among scenes compared to similarity among objects (Figure 3).

It is difficult to know how these and other possible differences in low-level stimulus properties among these two image categories might be responsible for the pattern of results seen in Figure 2. What is needed is a means for equalizing object and scene images while preserving their unique identities. This was the motive for development of the procedure described and tested in the next section.

Experiment 2: Comparison of CFS masks animated with normal or scrambled pointillist images of objects or scenes

We developed an image generation technique that closely matches spectral power distributions of images while maintaining their distinct figural appearances. As mentioned earlier, the technique was inspired by the pointillism format developed by George Seurat, wherein small dots of uniform color perceptually coalesce to portray recognizable global forms. In our version, images of objects and scenes are used as "seed" images that determine the colors of dots scattered over a canvas of the same size as the seed image. We created a large number of these pointillist images from the same sets of object and scene images used in Experiment 1, and then animated a long series of them by showing one after another at 9.375 Hz.

Pointillist image technique

A pointillist image is made from a set of dots and a seed image that determines the colors of dots (see

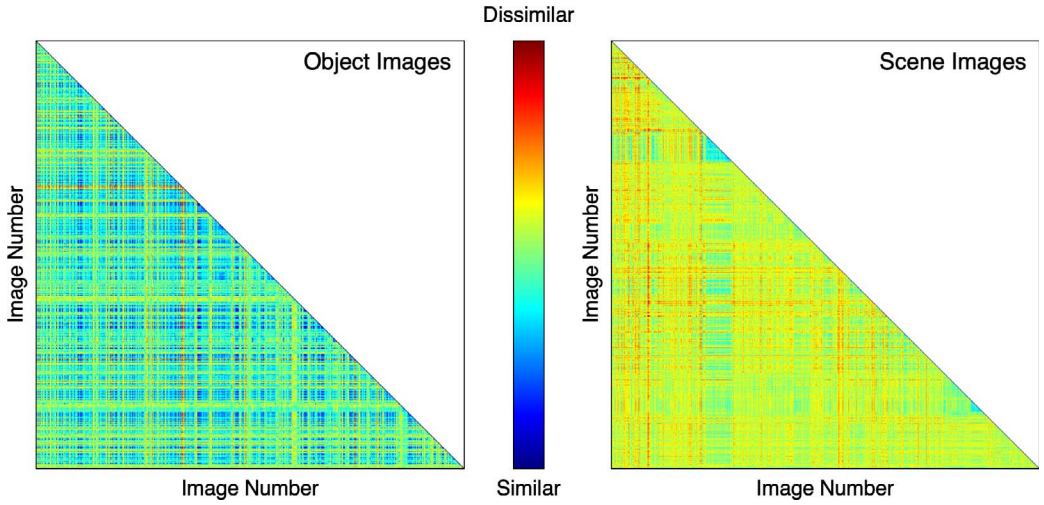

Figure 3. Dissimilarity matrices of the entire set of object images (left panel) and the entire set of scene images (right panel) used in Experiment 1. Dissimilarity between two images is defined as the average RGB distance of every pixel inside the circular aperture. Dissimilarity between the same images (i.e., minimum dissimilarity) is thus 0, and at its maximum the dissimilarity value can be a cube root of 3 ($1 + 1 + 1$, each for red, green, and blue luminance differences).

Figure 5 for examples of pointillist images). First, dots of various sizes are placed randomly over a canvas of the same size as the seed image. Dot sizes and locations are constrained to prohibit them from touching one other. The color of a given dot corresponds to the color portrayed in the seed image at the location of the center of each dot. For our displays, we placed 630 dots over a circular canvas of 200 pixels (4.40°) in diameter. One third of the dots had a diameter of 5 pixels (0.11°), another third had a diameter of 4 pixels (0.09°), and the other third had a diameter of 3 pixels (0.07°). We placed larger dots first and then smaller dots among larger dots to generate a denser array. We created 1,000 sets of 630 dots for each participant and used these sets to create pointillist images. As an aside, our technique could be construed as a variant of the "bubbles" technique introduced by Gosselin and Schyns (2001) for the study of object recognition and the salient features that support it. But their aim was exactly the opposite of ours: they sought to degrade recognition by sparsely sampling images seen within a relatively few blurred portions of it, whereas we sought to promote good image recognition by dense sampling of the images.

Figure 5 shows examples of the pointillist images together with the seed images, used in Experiment 1, from which those pointillist images were created. One ostensible advantage to this technique is that the local visual properties defined by the dots are approximately equal among pointillist images: images are comprised of the same number of dots with the same limited range of diameters, thereby ensuring that all images are identical in their area of stimulus and total contour content. In terms of spatial frequency and orientation, this conversion equates spectral power distributions and their variance in the spatial frequency range higher than the spatial frequency associated with the average size of the dots, while preserving the global pattern

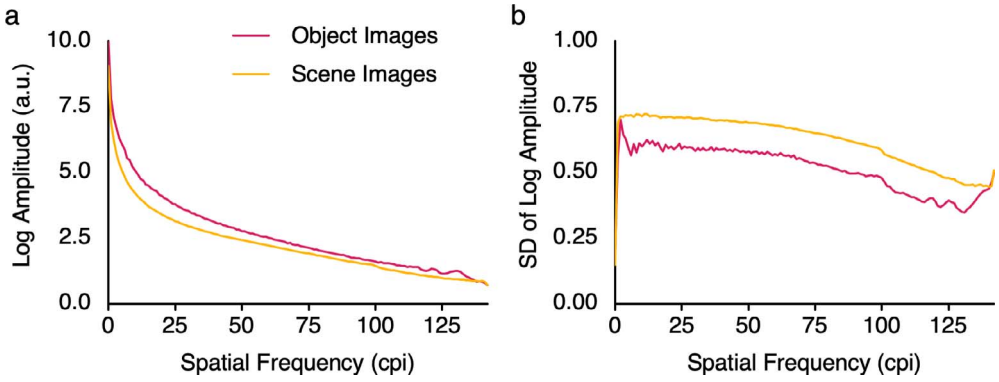

Figure 4. Average amplitude spectra (a) and variance of contrast energy in the amplitude spectra (b) for object images and scene images.

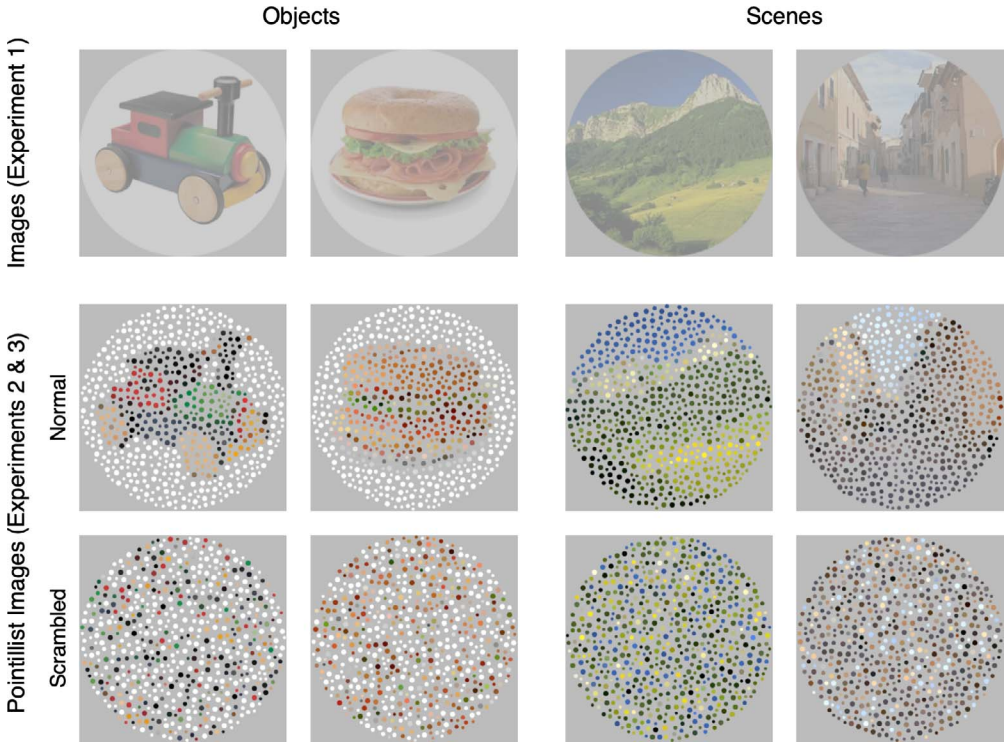

Figure 5. Examples of images comprising continuous flash suppression (CFS) sequences. The top row shows exemplars from the object/scene image database, the middle row shows pointillist images made from the exemplars in the top row, and the bottom row shows scrambled pointillist images made by randomly relocating dots from the pointillist images in the middle row. See Supplementary Movies S1–S4 for examples of object and scene animations—normal and scrambled.

embedded in the lower spatial frequency range (Figure 6). This technique also removes traces of small objects in the scene images thereby placing emphasis on their spatial layout per se. In our experiments, the average dot size was 4 pixels and the seed images extended 200 × 200 pixels. Consequently, the global pattern embedded in spatial frequencies lower than 25 cpi (cycles per image) survives the conversion to a pointillist image, maintaining the visual impression of the objects and the scenes being depicted.

A second advantage provided by pointillist images is that they can be "scrambled" simply by relocating the constituent dots. On the bottom row of Figure 5 are examples of scrambled pointillist images used in Experiment 2. Since this scrambling procedure only changes the locations of dots, it does not influence the local visual properties; that is, the spectral power distribution in the high spatial frequency range. Only the global pattern embedded in the lower spatial frequency range will be disturbed (Figure 6a and 6b, differences between the solid red/yellow and dashed black lines). We believe this form of scrambling is a viable alternative to the conventional technique of phase-scrambling, wherein a visual image is decomposed into a set of sine-wave components of various orientations and spatial frequencies that are then randomized with respect to their relative locations. A phase-scrambled image has the same spectral energy as the original image in both high and lower spatial frequency ranges, and this, of course, destroys any hint of the image's original content. But it is impossible to know whether this destruction of image "legibility" is attributable to the degradation of global pattern or local visual properties. Perceptually, there are qualitative differences between an original image and its phase-scrambled counterpart: phase-scrambled images typically lack sharp edges and extended, homogeneous surface regions that define the spatial structure evident in the original images. Our version of scrambling preserves edges and surfaces of every dot in a pointillist image. The resulting image will have the same clear impression of discrete dots as well as approximately the same amount of energy as that contained in the original, unscrambled pointillist image.

Experimental design

We made four different types of CFS sequences from normal and scrambled pointillist images. Two types of CFS sequences were created from two sets of pointillist images, one comprising objects and the other scenes. The other two types of CFS sequences were created from two sets of scrambled pointillist images of objects

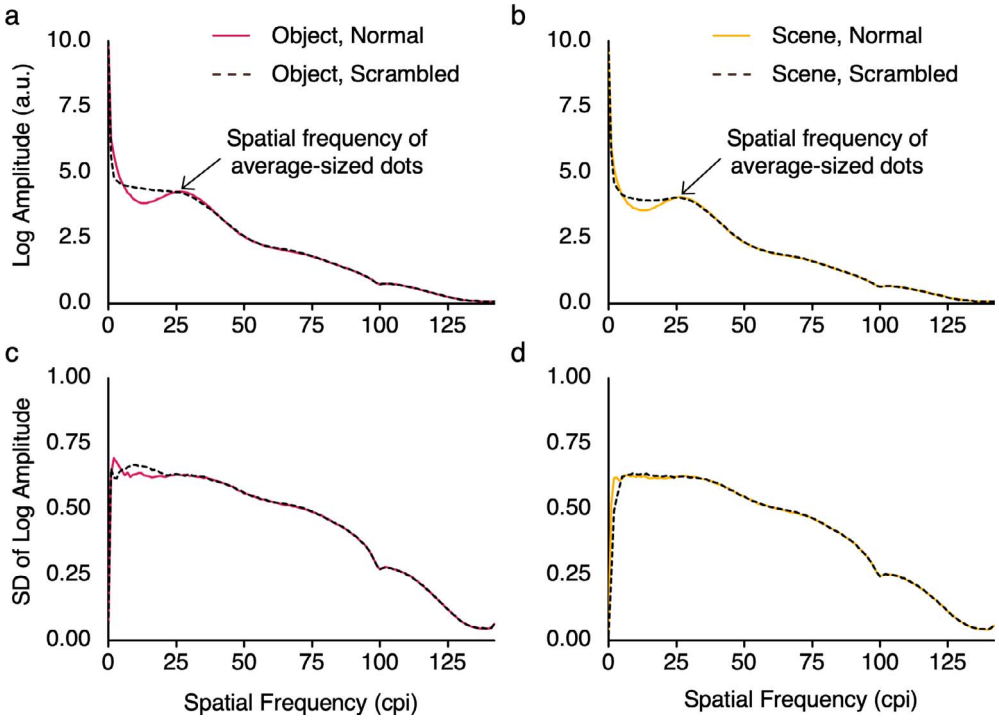

Figure 6. Average amplitude spectra of normal and scrambled pointillist images portraying objects (a) and scenes (b), and variance of contrast energy in the amplitude spectra of normal and scrambled pointillist images portraying objects (c) and scenes (d). Each image in the object/scene database was converted to a grayscale pointillist image (normal) that was also used to generate a scrambled version of that pointillist image. The amplitude spectra for each was derived, and the solid and dashed lines in (a) and (b) are the averages of those amplitude spectra. The solid and dashed lines in (c) and (d) are the variances of those amplitude spectra.

and of scenes. Note that CFS sequences of normal and scrambled pointillist images share the same visual elements (i.e., dots of the same colors) and thus, the only difference between the two is the recognizability of the image content. We compared BTs associated with those two CFS sequences, normal and scrambled. Prolonged suppression durations of the normal CFS sequences relative to the scrambled CFS sequences would implicate strengthened suppression caused by recognizable image content.

Methods

Participants

The same 10 participants who served in Experiment 1 participated in Experiment 2, again with informed consent and approval by the Institutional Review Board of Yonsei University. Again, we collected data from 10 participants, because this sample size showed very strong evidence (Bayes factor >150) in favor of the hypothesis of interest.

Stimuli and design

In Experiment 2, object and scene images were used as seed images to generate CFS sequences of pointillist images in the fashion described above (for the MATLAB code, see https://github.com/oakyoon/pretina-fabric). It is worth noting that approximately 73.75% of individual image pixels in these pointillist images constituted the background within which the windowed apertures appeared, and those background pixels were uniform gray. Thus, the overall RMS contrast values of the pointillist images was less than that of the original images, and the residual differences in RMS contrast among pointillist images were smaller.

In Experiment 2, we presented all four combinations of two classes of CFS masker stimuli (object and scene) and two types of CFS dot placements (normal and scrambled). Our aim was to determine BTs for each category of CFS mask. Over trials, the eye receiving the CFS mask and the eye receiving the target were counterbalanced over an irregular sequence. With 24 trials of repetition, the experiments consisted of 192 trials (object/scene $\times$ normal/scrambled $\times$ left eye/right eye $\times$ 24).

Procedure

The presentation sequence of the visual stimuli and participants' task were the same as in Experiment 1. The only exception was that the CFS displays consisted of pointillist images instead of images of low opacity.

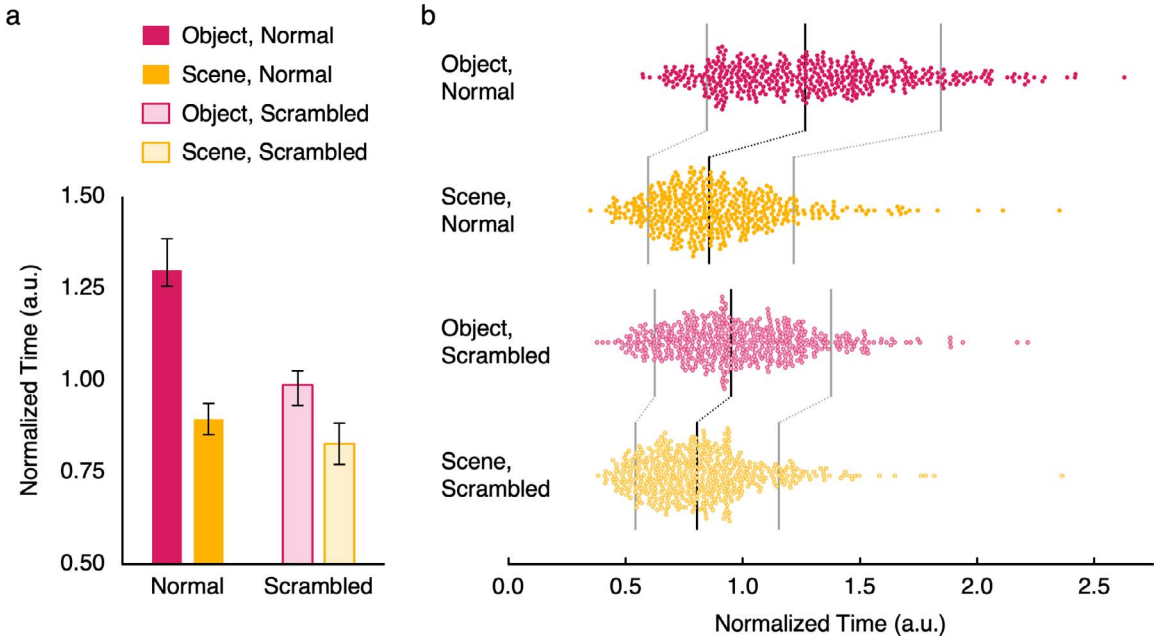

Figure 7. Results of Experiment 2. (a) The bar chart plots normalized breakthrough times (BTs) averaged over all participants, with error bars denoting 95% confidence intervals. (b) Shift-plot graphs show normalized BTs for every trial aggregated from all participants. Each dot represents one trial, black lines indicate 50th percentile, and gray lines indicate 10th and 90th percentiles.

Analysis

We analyzed our data using Bayesian repeated-measures ANOVA and reported BF_{10} for all models and $BF_{inclusion}$ for the effects of interest. First, we rejected the very infrequent trials on which a participant reported the incorrect direction of rotation of the target stimulus (*M*: 0.26%, *SD*: 0.51%) and the infrequent trials on which participants did not report seeing the target (*M*: 1.04%, *SD*: 1.75%). The average time required for participants to report the target motion direction (BT) in each condition was then divided by each participant's average BT in all conditions. These normalized BTs were used for further analyses.

Results and discussion

The average normalized durations required for the initially suppressed pinwheel target to break suppression (i.e., achieve perceptual dominance sufficient to make the two-alternative forced choice judgment of rotation direction) are shown in Figure 7a. In Figure 7b, those BTs for all trials for all participants in each of the four conditions (object vs. scene/normal vs. scrambled) are shown. Longer BTs in the normal condition relative to the scrambled condition imply stronger suppression attributable to the recognizable image content embedded in the normal pointillist images. Since our interest was in potential differences between CFS sequences of objects and CFS sequences of scenes, the statistical effect of interest in Experiment 2 was the interaction between the seed image (object vs. scene) and dot placements (normal vs. scrambled). Bayesian repeated-measures ANOVA identified the model including the interaction as the best model ($BF_{10} = 1.174 \times 10^{11}$, see Table 1), and $BF_{inclusion}$ for the interaction term was 259.4, indicating that the model with the interaction term was much more likely than models without the interaction term. These results are consistent with the conclusion that the nature of the image content of CFS masker stimuli can impact the strength of interocular suppression created by that masker. Pointillist images of objects presented in rapid sequence to one eye more effectively maintain suppression of a rotating pinwheel target presented to the other eye than do CFS sequences comprising pointillist images of scenes.

To our surprise, CFS masks comprising scrambled pointillist images of objects also produced more robust suppression than did CFS masks comprising scrambled pointillist images of scenes (compare light red and light yellow bars in Figure 7a). The magnitude of the differences in CFS potency are quite small for the scrambled object and scene images compared to the robustness of unscrambled objects and scenes (dark and light yellow bars in Figure 7a). Still, this result is puzzling and led us to wonder whether these potency differences between pointillist masks comprised of objects and of scenes might have something to do with differences in stimulus strength, not just

Model comparison		Analysis of effects	
Models	BF_{10}	Effects	$BF_{inclusion}$
Seed image	55,867.154	Seed image	2.154×10^7
Dot placements	20.009	Dot placements	8099.7
Seed image + dot placements	4.525×10^8	Seed image × dot placements	259.4
Seed image + dot placements + seed image × dot placements	1.174×10^{11}		

Table 1. Bayesian repeated-measures ANOVA results of BTs in Experiment 2.

content. The resemblance of the spectral power distributions in Figures 6a and 6b imply that the two types of images have comparable spatial frequency content, but, in fact, those spectra were derived using grayscale versions of the pointillist images, not colored images like the ones used in Experiment 2. Moreover, the spectral power distributions of normal and scrambled object pointillist images reveal slightly more energy compared to the spectra of normal and scrambled scene pointillist images. From other work (Ludwig, Sterzer, Kathmann, & Hesselmann, 2016), we know that contrast can influence CFS robustness. We thus felt obliged to repeat Experiment 2 using CFS masks comprising *grayscale* pointillist images derived from seed images *matched* in RMS contrast for both stimulus categories, object and scenes. All procedural aspects of this replication were identical to those used in Experiment 2—the only difference was that all CFS masks used in this replication utilized grayscale pointillist and scrambled images each constructed from seed images of objects and scenes that were rendered identical in RMS contrast (18%) and average luminance (34.03 cd/m^2, 40% of the maximum luminance; see Figure 8).

Results from this replication are shown in Figure 9. Comparing Figures 7 and 9, one sees that the results from this replication using pointillist grayscale images match the pattern of results found using colored pointillist images: once again, Bayesian repeated-measures ANOVA identified the model including the interaction term as the best model ($BF_{10} = 2.289 \times 10^{10}$), and including the interaction term increased the likelihood across matched models ($BF_{inclusion} = 8.075$).

Still, despite using contrast-matched images, we again find that scrambled pointillist images derived from objects produce more robust interocular suppression than do scrambled pointillist images derived from scene images (light red vs. light yellow bars in Figure 9a). Evidently there remains some residual difference between object and scene images that survives the image processing steps summarized in Figure 8: grayscale rendering, contrast normalization, discrete spatial sampling, and dot location scrambling. One such property is the luminance histogram summarizing the incidence of different luminance values of pixels within an image. The pattern embedded in a luminance histogram will survive the image transformations shown in Figure 8, perhaps comprising the residual responsible for the relative potency of scrambled pointillist objects compared to scrambled pointillist scenes (Figure 9a). The existence of this residual would also underscore why the appropriate statistical term is the interaction between image types (object and scene) and image structure (unscrambled and scrambled).

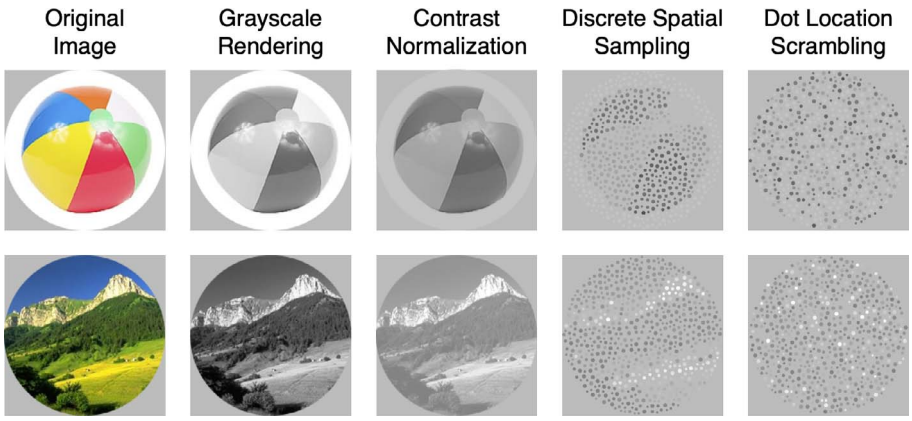

Figure 8. Series of transformations for converting an image to a contrast-matched grayscale pointillist image. Resulting normal and scrambled pointillist images (i.e., images in the rightmost two columns) were used for the replication of Experiment 2.

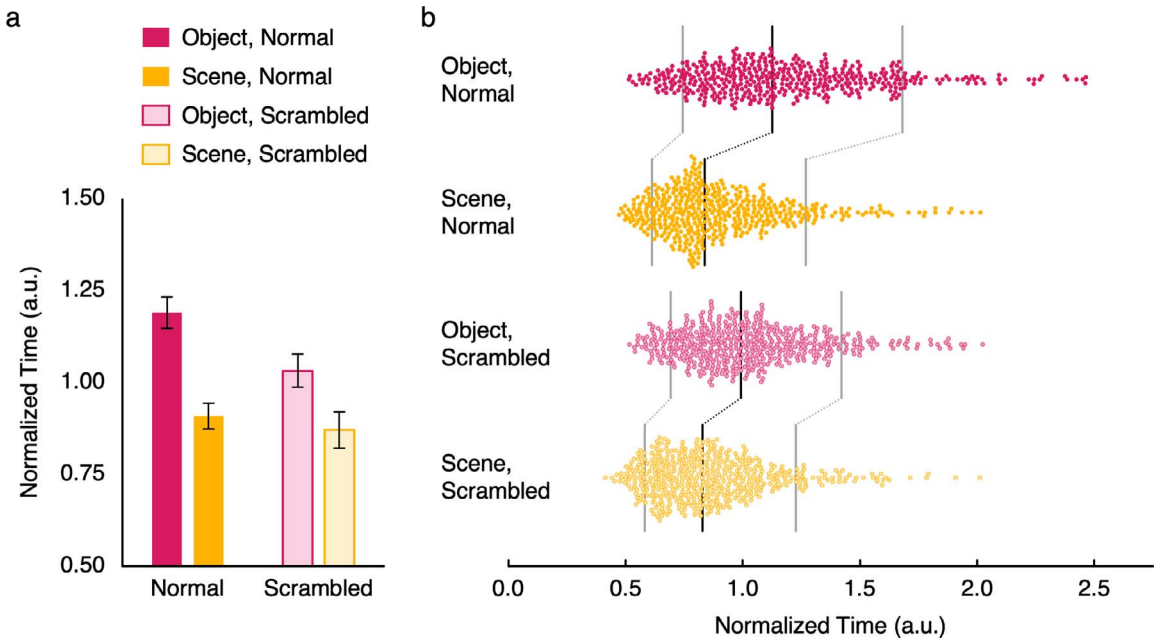

Figure 9. Results from the replication of Experiment 2 using grayscale pointillist images. (a) The bar chart plots normalized breakthrough times (BTs) averaged over all 10 participants (six of whom participated in the color version of Experiment 2), with error bars denoting 95% confidence intervals. (b) Shift-plot graphs show normalized BTs for every trial aggregated from all participants. Each dot represents one trial, black lines indicate 50th percentile, and gray lines indicate 10th and 90th percentiles.

Experiment 3: Durations for pointillist image sequences to regain perceptual dominance

In the first two experiments, we focused on the time required for a simple target stimulus (i.e., a rotating pinwheel) to gain dominance depending on the image content of the CFS masker (objects vs. scenes). In Experiment 3, we asked the complimentary question: Does the time required for a pointillist image sequence to achieve dominance when those sequences were initially suppressed by the simple target stimulus depend on the image content of the initially suppressed CFS sequence? This question, in other words, is formulated in the same way as earlier CFS studies of processing outside of awareness.

Methods

Participants

The same 10 participants tested in Experiments 1 and 2 participated in Experiment 3.

Apparatus

Apparatus and stimuli were the same as in Experiment 2.

Procedures

In Experiment 3, we changed the time course of contrast change of the pinwheel target, the purpose being to promote initial dominance of the target. Each trial began with the appearance of the fusion stimuli and fixation point, and the participant again pressed the spacebar to initiate the sequence of events illustrated in Figure 10. Initially, the pointillist image sequence (the same as a CFS sequence in Experiment 2) appeared but then 600 ms later the pinwheel target appeared abruptly at full contrast (100%), which usually triggered its immediate dominance. After its appearance, the contrast of the pinwheel target decreased smoothly, and the target completely disappeared after 9.4 s from its appearance. The decrease in contrast of the target C at a given time t was determined by the following formula: $C(t) = \log_{10}(10 - 9 \times (t - 0.6) \div 9.4)$. At the same time, its direction of rotation changed unpredictably every few seconds—the participant's task was to press one of two arrow keys to indicate the last perceived direction of rotation as soon as the target became imperceptible. With this sequence of stimulus events, participants could clearly perceive the presence and rotation direction of the pinwheel during the initial moments of the trial, but at some point the pointillist CFS sequence achieved exclusive dominance making it impossible to report rotation direction. On a few occasions, participants failed to perceive the pinwheel upon its immediate onset, in

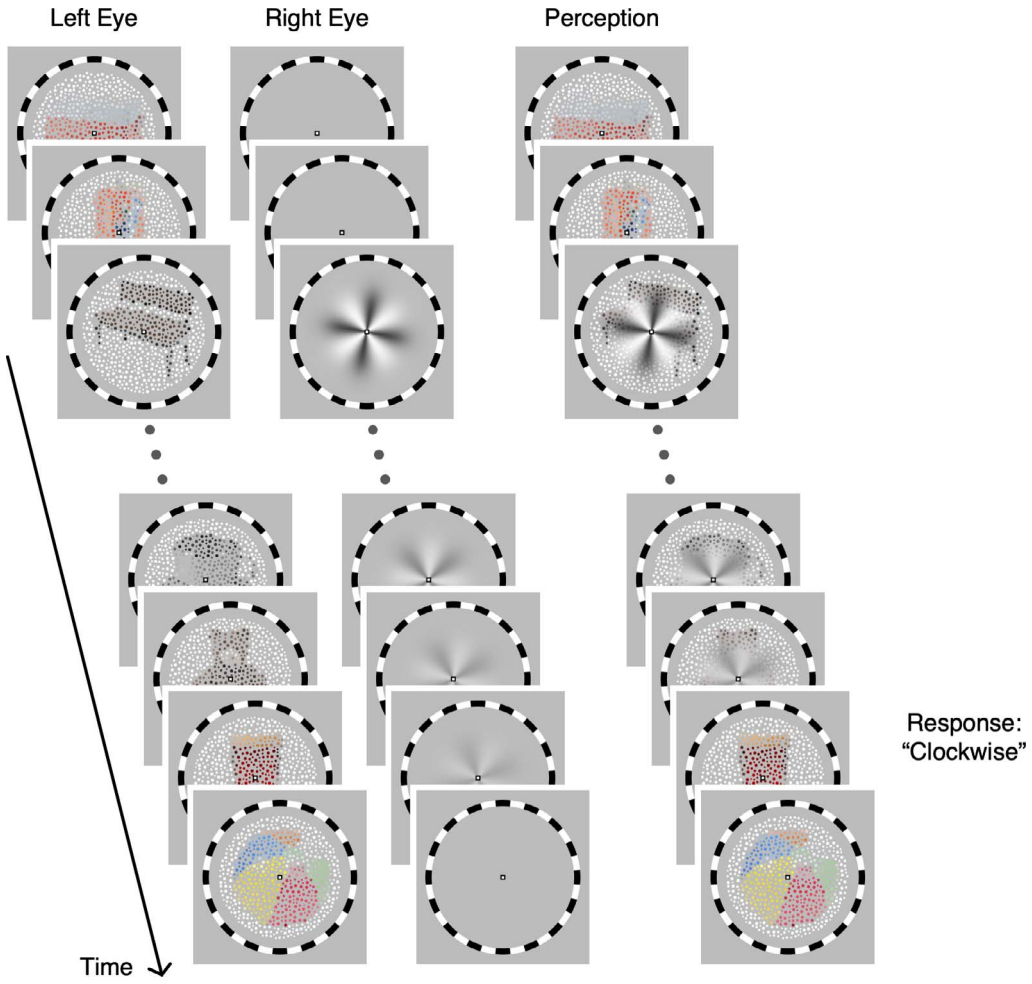

Figure 10. Procedures of Experiment 3. On each trial, two different image sequences were presented to the left and right eyes. In one eye's view, normal/scrambled pointillist images made from object/scene images were replaced at the rate of 9.375 Hz. In the other eye's view, a rotating pinwheel grating appeared at full contrast and then its contrast decreased over time. On most but not all trials, the abrupt onset of the high contrast grating promoted its immediate dominance. The rotation direction of the pinwheel changed unpredictably every few seconds, and participants reported the last direction of rotation perceived just before the grating succumbed to suppression.

which case they pressed a designated key to abort that trial.

Before formal data collection on this task, a practice session was conducted to ensure that participants were familiar with the display sequence and that they understand the task.

Analysis

For Experiment 3, we separately analyzed the number of trials where participants reported that the pinwheel stimulus failed to obtain perceptual dominance at the beginning (M: 20.10%, SD: 14.19%). Then incorrect trials (M: 11.97%, SD: 7.41%) were rejected from the remaining trials. In each condition, the average time elapsing before the pinwheel stimulus became invisible (time to suppression, ST) was divided by each participant's average STs in all conditions. These normalized STs were used for further analyses.

Results and discussion

Average normalized STs are shown in Figure 11a, and the STs of all incidences of the pointillist image sequences regaining perceptual dominance are shown in Figure 11b. Note that the total number of incidences are different in each condition, because in some trials the pinwheel target failed to obtain perceptual dominance with abrupt onset. When analyzed by itself, effect of interest in Experiment 3 would be the interaction between the seed image and dot placements. Bayesian repeated-measures ANOVA identified the model with only seed image term as the best model ($BF_{10} = 900.976$; see Table 2), which is 2.816 times more

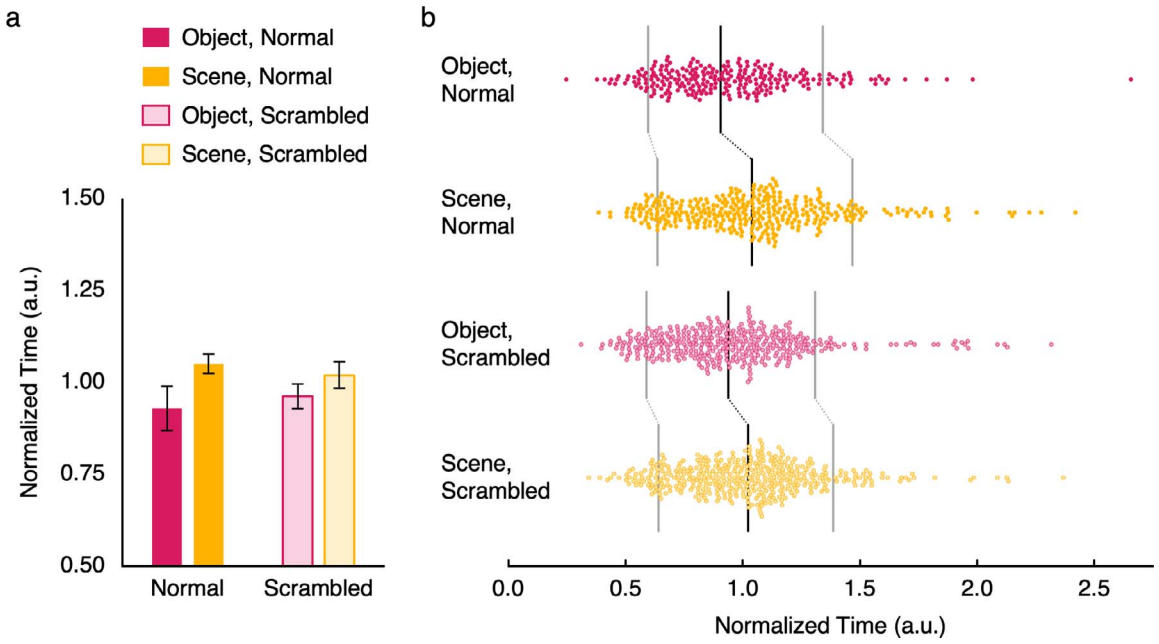

Figure 11. Results of Experiment 3. (a) The bar chart shows normalized breakthrough times (BTs) averaged over all participants, with error bars indicating 95% confidence intervals. (b) Normalized BTs for every trial aggregated from all participants are shown in shift-plot format, where each dot represents one trial, black lines indicate 50th percentile, and gray lines indicate 10th and 90th percentiles.

likely than the model with the interaction term (ratio between BF_{10} of the two models).

Next, we analyzed the data from Experiments 2 and 3 with experiment as a factor, as we were interested in whether the impact of the image content was weaker in Experiment 3. The effect of interest is the three-way interaction among experiment (Experiments 2 and 3), seed image, and dot placements. Bayesian repeated-measures ANOVA identified the model with the three-way interaction as the best model ($BF_{10} = 2.906 \times 10^{15}$), and $BF_{inclusion}$ for the three-way interaction term was 1,525.940. The impact of the image content of CFS masker was weak when those suppressed image sequences were struggling to displace the pinwheel target as the dominant one. These results suggest that the different potency of interocular suppression we found in Experiment 2 cannot be fully explained by the differences in spatio-temporal energy. Pointillist image sequences of objects had the same spatio-temporal energy in both Experiments 2 and 3. If those properties were responsible for increasing the breakthrough time of the pinwheel target, they should decrease the time for the object pointillist image sequences to regain perceptual dominance.

In addition, we analyzed the number of occasions when the pinwheel stimulus failed to obtain perceptual dominance despite its abrupt onset in Experiment 3. Bayesian repeated-measures ANOVA identified the model with the interaction between the seed image and dot placements as the best model ($BF_{10} = 391{,}351.114$), and $BF_{inclusion}$ for the interaction term was 50.750. Importantly, this pattern of results mirrors the finding from Experiment 2: CFS sequences comprising recognizable object pointillist images exerted much longer durations of interocular suppression in Experiment 2, and those same image sequences were more likely to resist the abrupt onset of the full-contrast pinwheel target (Experiment 3).

Model comparison		Analysis of effects	
Models	BF_{10}	Effects	$BF_{inclusion}$
Seed image	900.976	Seed image	894.793
Dot placements	0.305	Dot placements	0.296
Seed image + dot placements	266.446	Seed image × dot placements	1.201
Seed image + dot placements + seed image × dot placements	319.963		

Table 2. Bayesian repeated-measures ANOVA results of STs in Experiment 3.

General discussion

CFS masks consisting of sequence of images displaying different objects produce more robust interocular suppression than do sequences of images of different scenes, as evidenced by the durations of suppression those masks impose on of a rotating radial grating viewed by the other eye. This boost in CFS robustness engendered by object-based masks is found even when CFS arrays comprise pointillist-type portrayals of objects and scenes in which the RMS contrast and spatial frequency content are approximately equivalent. However, we found no evidence that suppression durations of CFS masks themselves vary with their image content: object- and scene-based CFS arrays exhibited comparable durations of suppression, although object-based CFS arrays were more resistant to suppression in the first place.

How do these findings compare to those from previous studies using CFS? To our knowledge, all of those previous studies manipulated the figural characteristics of the stimulus undergoing suppression by CFS masking, not the figural characteristics of the CFS mask itself. For example, Almeida et al. (2008) reported that pictures of tools remained effective as visual primes even when suppressed by CFS, whereas pictures of animals were rendered ineffective as primes by CFS. They attributed this category-specific effect of CFS to the differential impact of interocular suppression on dorsal versus ventral stream visual processing (cf. Fang & He, 2005). Results from subsequent studies (Almeida, Mahon, & Caramazza, 2010; Sakuraba et al., 2012), however, provided a somewhat different twist on that conclusion by focusing on low-level surface and shape characteristics of visual images (e.g., elongation) that distinguish tools versus animals. These are just a few examples of the multiple studies that have yielded mixed results concerning the propensity for certain categories of visual targets to escape CFS masking more quickly than control stimuli. Comprehensive reviews of those studies are provided by Ludwig and Hesselmann (2015) and by Moors et al. (2016). Our Experiment 3 is somewhat comparable to those earlier CFS studies in that we did ask whether STs differed for pointillist image sequences of objects compared to pointillist image sequences of scenes, and we found no differences between those two categories of pointillist animations. We did, however, observe that pointillist image sequences portraying objects were more resistant to initial suppression than were pointillist image sequences of scenes. This is a potentially revealing finding that we return to later in this discussion.

What about the results of Experiments 1 and 2, where we adopted the complimentary approach of manipulating the characteristics of the arrays of images comprising the CFS mask that induced suppression? As Figures 2, 7, 9, and 11 document, we do find robust differences in the propensity for object- versus scene-based CFS animations to maintain suppression of a test target. However, it is not straightforward to compare those results to findings from the earlier CFS studies of selective stimulus processing outside of awareness. For one thing, earlier studies have presented a single category, unchanging exemplar to one eye for the entire duration of a trial, a procedure that allows time for accumulation of information about that particular suppressed exemplar. With our technique, a given category condition involved rapid changes in the exemplars of that category, minimizing accumulation of information about any single target exemplar during a trial. We made no effort to constrain the particulars of the exemplars comprising a given object-based CFS (e.g., images could include graspable, nongraspable, animate, or inanimate exemplars), nor were constraints placed on the particulars of the exemplars of the scenes (e.g., man-made scenes, urban vs. natural landscapes). In other words, we created those image sequences purposefully to focus on global properties that potentially distinguish objects from scenes, without reference to the specific features or affordances that define a given image. Moreover, we employed only a single type of test figure in Experiments 1 and 2 (i.e., a rotating radial grating). We purposefully did that for two reasons: (a) to minimize potential confusion on the part of participants about what they might see upon the target's emergence from suppression, and (b) to create a forced-choice response task (CW vs. CCW rotation) to be performed by participants as a proxy for simply deciding when the target was visible. It is reasonable to wonder, however, to what extent the object/scene differences in CFS potency might vary depending on the nature of the target being suppressed.

Turning to our results themselves, why do CFS animations comprising object exemplars produce longer durations of interocular suppression than do CFS animations comprising scene exemplars? This was found with unmanipulated color images of objects and scenes (Figure 2), pointillist versions of those images (Figure 7), and contrast-matched grayscale versions of those pointillist images (Figure 9). What empowers CFS comprised of images of objects relative to CFS comprised of images of scenes?

To tackle that question, we first turned to the literature on object and scene recognition and its dependence on low-level features, specifically spatial frequency (Morrison & Schyns, 2001; Schyns & Oliva, 1997). For the kind of viewing situation we have created—different images presented every 100 ms with no explicit identification task—a number of lines of evidence suggest that images of objects and of scenes are processed in a coarse-to-fine manner, with low spatial frequency signals predominating with brief

exposures (reviewed in Schyns & Oliva, 1994). As seen in Figure 6a and 6b, the low spatial frequency regions of the spectra of unscrambled pointillist images exhibit a localized dip in the power associated with those images, centered at approximately 12.5 cpi; no such dip is seen in the scrambled pointillist images. On the face of it, this localized reduction in contrast energy seems paradoxical because scrambled images are, in fact, *less* effective compared to their unscrambled counterparts when it comes to exerting CFS. Moreover, this dip in power is comparable in object and in scene images, yet object images beget more robust CFS. In other words, if low spatial frequencies were advantaged in our CFS arrays, we would expect an entirely different pattern of results from what is seen in Figure 9. We are not saying that our findings disagree with a coarse-to-fine analysis when it comes to processing of objects and scenes, but differences in spatial frequency energy alone do not account for the differential efficacy of those two categories of images when they comprise CFS masks. In other work using different CFS sequences, we are currently exploring this peculiar pattern of results.

As another possible explanation for the robustness of interocular suppression produced by object-based CFS masks compared to scene-based CFS masks, one could suppose that (a) visual information about objects and about scenes is processed within different networks of visual areas, and (b) that those networks are not equally impacted by the competitive neural interactions responsible for interocular suppression. From human brain imaging studies, there is good evidence for the first supposition. As elaborated elsewhere (Harel et al., 2013; Kamps et al., 2016; Kravitz et al., 2011), there appear to exist gradients of object and spatial layout information formed by interactions within areas in the ventral and parietal lobe that differ in neural responsiveness to objects and to spatial layout. But as for the second supposition, previous brain imaging studies using object images and place images as rival stimuli found robust interocular suppression in neural activity in both object- and scene-selective areas within ventral stream regions selectively activated by those images (Sterzer et al., 2008; Tong, Nakayama, Vaughan, & Kanwisher, 1998). Perhaps a more fine-grained examination of neural activity during interocular suppression within the gradients now thought to distinguish object and scene information might lead to refinement of the conclusions from those two extant studies, both of which used faces and houses as the "object" and "place" exemplars.

It is natural to ask whether the differential impact of objects relative to scenes in terms of inducing interocular suppression might arise from systemic structural differences between object and scene images. All of the object images in the library we used contain a single item whose surface regions are contiguous and appear against a uniform background; the scene images, on the other hand, typically comprise larger surface areas defined by ground, sky, or sea, and those larger surfaces tend to have subtler gradients of color and shading compared to the surfaces comprising object images. As a consequence, pointillist images portraying objects, compared to scenes, tend to have more discrete, colorful clusters of dots and clearer delineations between neighboring clusters. Perhaps, then, these properties enhance the visual salience and/or recognizability of objects, including pointillist images of objects. Those differences would not necessarily be reflected in the 2D spatial frequency amplitude spectra, but they could emerge from image analyses that isolate higher-order, structural characteristics supporting figure/ground segmentation and grouping, perceptual operations engaged in natural viewing situations whenever we focus on an object or more broadly take in a scene.

To explore whether stimulus salience might offer an explanation for our results, we tried deriving salience maps using the technique developed by Itti and colleagues (Itti, Koch, & Niebur, 1998; MATLAB implementation by Harel, Koch, & Perona, 2007). This is a bottom-up, data-driven model that derives metrics of salience based on parallel computations within topographic feature maps representing orientation, color, and luminance in multiple spatial scales. But with pointillist images, fine-scale visual information is governed by visual properties of the dots themselves: orientation information is dominated by the circular apertures and the contrast information is strongly dependent on the dots' color and lightness values relative to the uniform gray background. Consequently, the average salience map for objects looks no different from the average map for scenes. When viewing pointillist images, a person readily discounts the saliency of visual properties associated with dots' apertures once they realize that visual meaning is embedded in the patterns of the dots. Bottom-up, data-driven models of salience, however, are not designed to include this kind of top-down information. (This is not to say, however, that attention is not a cause of the relative robustness of objects compared to scenes, a point we return to below.)

Next, we considered whether images of objects might be more recognizable than images of scenes when each image was viewed for a fraction of a second in a steady stream of different images. From earlier work on binocular rivalry, we know that a recognizable stimulus enjoys greater predominance than does an unrecognizable one (Yu & Blake, 1992; Baker & Graf, 2009). If CFS potency, too, is influenced by recognizability, one could surmise that objects are more potent suppressors because they are easier to recognize than are scenes. The original images used in our study were selected

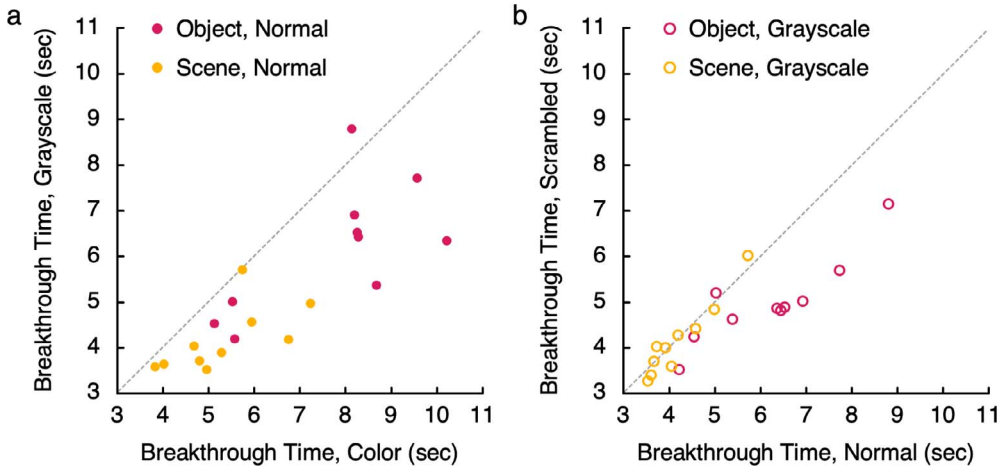

Figure 12. Results of the replication using grayscale pointillist images. (a) Each dot plots the average breakthrough time (BT) for a participant measured for a mask type (normal object or normal scene pointillist images). The *x*- and *y*-axes represent BTs in the color (Experiment 2) and in the grayscale Experiments, respectively. Note that (a) BTs for object sequences are generally longer than BTs for scene sequences, and (b) that nearly all BT values fall below the unity line (i.e., are longer for color vs. grayscale image sequences). (b) Each dot plots the average BT for a participant measured for a mask type (object or scene pointillist images) in the grayscale Experiment. The *x*- and *y*-axes represent BTs for the normal and scrambled pointillist image sequences, respectively. Note that yellow outlined dots (BTs for the scene pointillist image sequences) are on or near the unity line, showing that BTs are similar for the normal and scrambled grayscale scene pointillist image sequences.

from widely used image libraries of objects and of scenes, but we did not assess image recognition under the particular conditions of our experiments. However, we did manipulate those images in ways that plausibly impact the clarity of their content (i.e., converting the colored pointillist images into grayscale pointillist images). If that manipulation degrades recognizability, we would predict that grayscale object- and scene-based CFS sequences should be less effective than their color counterparts and, as a consequence, should yield shorter BT durations. That pattern of results would not be evident from comparison of the bar charts in Figures 7 and 9 because the BT durations in those figures are normalized for each observer and experiment and, moreover, the RMS contrasts differed between the color images and the grayscale contrast-matched images. So, instead, we analyzed the raw BT values produced by the object- and scene-based CFS sequences (Figure 7) to BTs measured in an exact replication of Experiment 2 using grayscale images identical in RMS contrast to the color images. We also tested the same 10 participants who performed the color pointillist task.

The raw BTs from those two sets of results clearly reveal the predicted pattern of results (Figure 12a): average BTs for colored, pointillist images of objects and of scenes were ~20% longer than were BTs produced by grayscale images identical in RMS contrast to their colored counterparts. Loss of color weakens the potency of images comprising CFS masks. Another revealing trend found in the raw BTs emerges from comparison of intact and scrambled grayscale images (Figure 12b). For grayscale scene images, BTs between intact and scrambled sequences are not significantly different ($BF_{10} = 0.326$), whereas for grayscale object images the BT differences between intact and scrambled remain significant ($BF_{10} = 3.509$). This is consistent with the hypothesis that the recognizability of scene images is more vulnerable to loss of color than is the recognizability of object images.

Whatever structural properties empower object-based CFS relative to scene-based CFS, those properties appear to be ineffective when it comes to hastening a transition from suppression to dominance: dynamic object CFS sequences exhibit the same suppression BTs as dynamic scene CFS sequences (Experiment 3). In this respect, the structural differences between object and scenes do not behave like contrast (e.g., Brascamp, Klink, & Levelt, 2015), luminance (e.g., Levelt, 1965), and spatial frequency complexity (e.g., Baker & Graf, 2009), early level visual properties that reliably modulate suppression durations. Returning to a point made above, the fact that object-based CFS sequences exert their greater strength when they are dominant but not when they are suppressed leads us to wonder whether their enhanced robustness may arise from their stronger engagement of visual attention, which is known to boost the strength of images during their dominance phases (Dieter, Brascamp, Tadin, & Blake, 2016; Ling & Blake, 2012; Stein et al., 2012).

There are certainly additional experiments one could envision for studying in more detail this difference between dynamic arrays of objects and dynamic arrays of scenes as potent CFS maskers. For instance, the pointillist image technique could be used to create multiple, independent versions of a given object or a given scene generated from a single seed image, thereby allowing one to portray a single exemplar (or it's scrambled counterpart) for an entire trial. Would such a dynamic mask be as effective as the series of images randomly selected from a category set? One could also determine what happens when a CFS mask consists of exemplars drawn from both of those two categories. Would that hybrid mask form a diluted version of a pure object-based CFS masker in terms of its suppressive potency? Do pointillist images of natural scenes (e.g., a forest) generate different levels of suppression than do pointillist images of scenes portraying man-made structures (e.g., urban landscapes) and, if so, are those differences traceable to image structure? What is found using CFS masks in which image recognition is degraded systematically by varying the density and/or sizes of the apertures defining the pointillist dots of color or luminance? Do pointillist images of upright faces induce stronger CFS masking than do masks comprised of inverted faces (Jiang et al., 2007)? Answering those and related questions is beyond the more modest aim of this paper, which was to introduce the pointillist technique for creating CFS sequences.

Going beyond interocular suppression and CFS, we foresee that that pointillist images could also be useful in studying other visual tasks where matches among a succession of images are required over time (apparent motion) or over space between the two eyes (left- and right-eye images in which retinal disparity supports stereopsis). The pointillism technique has value because it does a good job of approximately matching the spatial frequency content of diverse images drawn from different stimulus categories while preserving configural information that gives those images visual meaning. We can envision utilizing pointillist images for training and testing generalization of image categorization by convolutional neural networks (CNNs). A recent study has shown that CNN models trained only on local features, without regard to their global configuration, rival the classification rates of ImageNet trained CNNs (Brendel & Bethge, 2019). Given our ability to seamlessly recognize the objects in a Seurat painting, a CNN capable of classifying pointillist images, devoid of local feature differences, would bolster current efforts to develop CNNs that mimic the human biological visual system (Cichy, Khosla, Pantazis, Torralba, & Oliva, 2016; Khaligh-Razavi & Kriegeskorte, 2014; Yamins & DiCarlo, 2016).

Keywords: continuous flash suppression, interocular suppression, pointillism, image processing, objects, scenes

Acknowledgments

This work was supported by NIGMS of the National Institutes of Health under award number T32GM007347, by a National Research Foundation of Korea (NRF) grant funded by the Korean government (MSIT; NRF-2016R1A2B4016171), and by the Centennial Research Fund awarded by Vanderbilt University. We thank Sonia Poltoratski, Aude Oliva, and Isabel Gauthier for helpful discussions about aspects of this project, and the two anonymous referees whose comments on our initial submission were very helpful in framing this version.

Commercial relationships: none.
Corresponding author: Randolph Blake.
Email: randolph.blake@vanderbilt.edu.
Address: Department of Psychology, Vanderbilt University, Nashville, TN, USA.

References

Abir, Y., Sklar, A. Y., Dotsch, R., Todorov, A., & Hassin, R. R. (2018). The determinants of consciousness of human faces. *Nature Human Behaviour*, *2*, 194–199, https://doi.org/10.1038/s41562-017-0266-3.

Almeida, J., Mahon, B. Z., & Caramazza, A. (2010). The role of the dorsal visual processing stream in tool identification. *Psychological Science*, *21*(6), 772–778, https://doi.org/10.1177/0956797610371343.

Almeida, J., Mahon, B. Z., Nakayama, K., & Caramazza, A. (2008). Unconscious processing dissociates along categorical lines. *Proceedings of the National Academy of Sciences, USA*, *105*(39), 15214–15218, https://doi.org/10.1073/pnas.0805867105.

Baker, D. H., & Graf, E. W. (2009). Natural images dominate in binocular rivalry. *Proceedings of the National Academy of Sciences, USA*, *106*(13), 5436–5441, https://doi.org/10.1073/pnas.0812860106.

Barrett, L. F. (2018). Seeing fear: It's all in the eyes? *Trends in Neurosciences*, *41*(9), 559–563, https://doi.org/10.1016/j.tins.2018.06.009.

Blake, R., Goodman, R., Tomarken, A., & Kim, H. W. (2019). Individual differences in continuous flash suppression: Potency and linkages to binocular rivalry dynamics. *Vision Research*, *160*, 10–23, https://doi.org/10.1016/j.visres.2019.04.003.

Brainard, D. H. (1997). The psychophysics toolbox. *Spatial Vision*, *10*(4), 433–436.

Brascamp, J. W., Klink, P. C., & Levelt, W. J. (2015). The "laws" of binocular rivalry: 50 years of Levelt's propositions. *Vision Research*, *109*, 20–37, https://doi.org/10.1016/j.visres.2015.02.019.

Breitmeyer, B. G. (2015). Psychophysical "blinding" methods reveal a functional hierarchy of unconscious visual processing. *Consciousness & Cognition*, *35*, 234–250, https://doi.org/10.1016/j.concog.2015.01.012.

Brendel, W., & Bethge, M. (2019, May). *Approximating CNNs with bag-of-local-features models works surprisingly well on ImageNet*. International Conference on Learning Representations (ICLR).

Chiesa, P. A., Liuzza, M. T., Acciarino, A., & Aglioti, S. M. (2015). Subliminal perception of others' physical pain and pleasure. *Experimental Brain Research*, *233*(8), 2373–2382, https://doi.org/10.1007/s00221-015-4307-8.

Cichy, R. M., Khosla, A., Pantazis, D., Torralba, A., & Oliva, A. (2016). Comparison of deep neural networks to spatio-temporal cortical dynamics of human visual object recognition reveals hierarchical correspondence. *Scientific Reports*, *6*: 27755, https://doi.org/10.1038/srep27755.

Dienes, Z. (2011). Bayesian versus orthodox statistics: Which side are you on? *Perspectives on Psychological Science*, *6*(3), 274–290, https://doi.org/10.1177/1745691611406920.

Dieter, K. C., Brascamp, J., Tadin, D., & Blake, R. (2016). Does visual attention drive the dynamics of bistable perception? *Attention, Perception, & Psychophysics*, *78*(7), 1861–1873, https://doi.org/10.3758/s13414-016-1143-2.

Doi, H., & Shinohara, K. (2016). Emotional faces influence numerosity estimation without awareness. *Cognitive Processing*, *17*(4), 389–397, https://doi.org/10.1007/s10339-016-0774-5.

Eo, K., Cha, O., Chong, S. C., & Kang, M.-S. (2016). Less is more: Semantic information survives interocular suppression when attention is diverted. *Journal of Neuroscience*, *36*(20), 5489–5497, https://doi.org/10.1523/JNEUROSCI.3018-15.2016.

Fang, F., & He, S. (2005). Cortical responses to invisible objects in the human dorsal and ventral pathways. *Nature Neuroscience*, *8*(10), 1380–1385, https://doi.org/10.1038/nn1537.

Gayet, S., & Stein, T. (2017). Between-subject variability in the breaking continuous flash suppression paradigm: Potential causes, consequences, and solutions. *Frontiers in Psychology*, *8*:437, https://doi.org/10.3389/fpsyg.2017.00437.

Gayet, S., Van der Stigchel, S., & Paffen, C. L. (2014). Breaking continuous flash suppression: Competing for consciousness on the pre-semantic battlefield. *Frontiers in Psychology*, *5*:460, https://doi.org/10.3389/fpsyg.2014.00460.

Gosselin, F., & Schyns, P. G. (2001). Bubbles: A technique to reveal the use of information in recognition tasks. *Vision Research*, *41*(17), 2261–2271, https://doi.org/10.1016/S0042-6989(01)00097-9.

Gray, K. L. H., Adams, W. J., Hedger, N., Newton, K. E., & Garner, M. (2013). Faces and awareness: Low-level, not emotional factors determine perceptual dominance. *Emotion*, *13*(3), 537–544, https://doi.org/10.1037/a0031403.

Han, S., & Alais, D. (2018). Strength of continuous flash suppression is optimal when target and masker modulation rates are matched. *Journal of Vision*, *18*(3):3, 1–14, https://doi.org/10.1167/18.3.3. [PubMed] [Article]

Han, S., Lunghi, C., & Alais, D. (2016). The temporal frequency tuning of continuous flash suppression reveals peak suppression at very low frequencies. *Scientific Reports*, *6*: 35723, https://doi.org/10.1038/srep35723.

Harel, J., Koch, C., & Perona, P. (2007). Graph-based visual saliency. In B. Schölkopf, J. C. Platt, & T. Hoffman (Eds.), *Advances in neural information processing systems* (pp. 545–552). Cambridge, MA: MIT Press.

Harel, A., Kravitz, D. J., & Baker, C. I. (2013). Deconstructing visual scenes in cortex: Gradients of object and spatial layout information. *Cerebral Cortex*, *23*(4), 947–957, https://doi.org/10.1093/cercor/bhs091.

Hedger, N., Gray, K. L., Garner, M., & Adams, W. J. (2016). Are visual threats prioritized without awareness? A critical review and meta-analysis involving 3 behavioral paradigms and 2696 observers. *Psychological Bulletin*, *142*(9), 934–968, https://doi.org/10.1037/bul0000054.

Hung, S.-M., Styles, S. J., & Hsieh, P.-J. (2017). Can a word sound like a shape before you have seen it? Sound-shape mapping prior to conscious awareness. *Psychological Science*, *28*(3), 263–275, https://doi.org/10.1177/0956797616677313.

Itti, L., Koch, C., & Niebur, E. (1998). A model of saliency-based visual attention for rapid scene analysis. *IEEE Transactions on Pattern Analysis and Machine Intelligence*, *20*(11), 1254–1259, https://doi.org/10.1109/34.730558.

Team. JASP (2018). JASP (Version 0.9.0.1) [Computer Software]. Available at https://jasp-stats.org/

Jiang, Y., Costello, P., Fang, F., Huang, M., & He, S. (2006). A gender- and sexual orientation-dependent

spatial attentional effect of invisible images. *Proceedings of the National Academy of Sciences, USA*, *103*(45), 17048–17052, https://doi.org/10.1073/pnas.0605678103.

Jiang, Y., Costello, P., & He, S. (2007). Processing of invisible stimuli: Advantage of upright faces and recognizable words in overcoming interocular suppression. *Psychological Science*, *18*(4), 349–355, https://doi.org/10.1111/j.1467-9280.2007.01902.x.

Kamps, F. S., Julian, J. B., Kubilius, J., Kanwisher, N., & Dilks, D. D. (2016). The occipital place area represents the local elements of scenes. *NeuroImage*, *132*, 417–424, https://doi.org/10.1016/j.neuroimage.2016.02.062.

Kang, M.-S., Blake, R., & Woodman, G. F. (2011). Semantic analysis does not occur in the absence of awareness induced by interocular suppression. *Journal of Neuroscience*, *31*(38), 13535–13545, https://doi.org/10.1523/JNEUROSCI.1691-11.2011.

Kaunitz, L., Fracasso, A., & Melcher, D. (2011). Unseen complex motion is modulated by attention and generates a visible aftereffect. *Journal of Vision*, *11*(13):10, 1–9, https://doi.org/10.1167/11.13.10. [PubMed] [Article]

Khaligh-Razavi, S. M., & Kriegeskorte, N. (2014). Deep supervised, but not unsupervised, models may explain IT cortical representation. *PLoS Computational Biology*, *10*(11): e1003915, https://doi.org/10.1371/journal.pcbi.1003915.

Kim, C.-Y., & Blake, R. (2005). Psychophysical magic: Rendering the visible "invisible". *Trends in Cognitive Sciences*, *9*(8), 381–388, https://doi.org/10.1016/j.tics.2005.06.012.

Kim, H.-W., Kim, C.-Y., & Blake, R. (2017). Monocular perceptual deprivation from interocular suppression temporarily imbalances ocular dominance. *Current Biology*, *27*(6), 884–889, https://doi.org/10.1016/j.cub.2017.01.063.

Konkle, T., Brady, T. F., Alvarez, G. A., & Oliva, A. (2010). Conceptual distinctiveness supports detailed visual long-term memory for real-world objects. *Journal of Experimental Psychology: General*, *139*(3), 558–578, https://doi.org/10.1037/a0019165.

Kravitz, D. J., Peng, C. S., & Baker, C. I. (2011). Real-world scene representations in high-level visual cortex: It's the spaces more than the places. *Journal of Neuroscience*, *31*(20), 7322–7333, https://doi.org/10.1523/JNEUROSCI.4588-10.2011.

Lapate, R. C., Rokers, B., Tromp, D. P. M., Orfali, N. S., Oler, J. A., Doran, S. T., … Davidson, R. J. (2016). Awareness of emotional stimuli determines the behavioral consequences of amygdala activation and amygdala-prefrontal connectivity. *Nature Scientific Reports*, *6*, 25826, https://doi.org/10.1038/srep25826.

Levelt, W. J. M. (1965). *On binocular rivalry*. Soesterberg, The Netherlands: Institute of Perception RVO-TNO.

Lin, Z., & He, S. (2009). Seeing the invisible: The scope and limits of unconscious processing in binocular rivalry. *Progress in Neurobiology*, *87*(4), 195–211, https://doi.org/10.1016/j.pneurobio.2008.09.002.

Ling, S., & Blake, R. (2012). Normalization regulates competition for visual awareness. *Neuron*, *75*(3), 531–540, https://doi.org/10.1016/j.neuron.2012.05.032.

Ludwig, K., & Hesselmann, G. (2015). Weighing the evidence for a dorsal processing bias under continuous flash suppression. *Consciousness & Cognition*, *35*, 251–259, https://doi.org/10.1016/j.concog.2014.12.010.

Ludwig, K., Sterzer, P., Kathmann, N., Franz, V. H., & Hesselmann, G. (2013). Learning to detect but not to grasp suppressed visual stimuli. *Neuropsychologia*, *51*(13), 2930–2938, https://doi.org/10.1016/j.neuropsychologia.2013.09.035.

Ludwig, K., Sterzer, P., Kathmann, N., & Hesselmann, G. (2016). Differential modulation of visual object processing in dorsal and ventral stream by stimulus visibility. *Cortex*, *83*, 113–123, https://doi.org/10.1016/j.cortex.2016.07.002.

Lunghi, C., Lo Verde, L., & Alais, D. (2017). Touch accelerates visual awareness. *i-Perception*, *8*(1): 2041669516686986, https://doi.org/10.1177/2041669516686986.

Maruya, K., Watanabe, H., & Watanabe, M. (2008). Adaptation to invisible motion results in low-level but not high-level aftereffects. *Journal of Vision*, *8*(11):7, 1–11, https://doi.org/10.1167/8.11.7. [PubMed] [Article]

Moors, P., Boelens, D., van Overwalle, J., & Wagemans, J. (2016). Scene integration without awareness: No conclusive evidence for processing scene congruency during continuous flash suppression. *Psychological Science*, *27*(7), 945–956, https://doi.org/10.1177/0956797616642525.

Moors, P., Hesselmann, G., Wagemans, J., & van Ee, R. (2017). Continuous flash suppression: Stimulus fractionation rather than integration. *Trends in Cognitive Sciences*, *21*(10), 719–721, https://doi.org/10.1016/j.tics.2017.06.005.

Morrison, D. J., & Schyns, P. G. (2001). Usage of spatial scales for the categorization of faces, objects, and scenes. *Psychonomic Bulletin & Review*, *8*(3), 454–469, https://doi.org/10.3758/BF03196180.

Mudrik, L., Breska, A., Lamy, D., & Deouell, L. Y. (2011). Integration without awareness: Expanding the limits of unconscious processing. *Psychological Science*, *22*(6), 764–770, https://doi.org/10.1177/0956797611408736.

Nuutinen, M., Mustonen, T., & Häkkinen, J. (2018). CFS MATLAB toolbox: An experiment builder for continuous flash suppression (CFS) task. *Behavior Research Methods*, *50*(5), 1933–1942, https://doi.org/10.3758/s13428-017-0961-z.

Oliva, A., & Torralba, A. (2001). Modeling the shape of the scene: A holistic representation of the spatial envelope. *International Journal of Computer Vision*, *42*(3), 145–175, https://doi.org/10.1023/A:1011139631724.

Peel, H. J., Sherman, J. A., Sperandio, I., Laycock, R., & Chouinard, P. A. (2019). Perceptual size discrimination requires awareness and late visual areas: A continuous flash suppression and interocular transfer study. *Consciousness & Cognition*, *67*, 77–85, https://doi.org/10.1016/j.concog.2018.11.012.

Pelli, D. G. (1997). The VideoToolbox software for visual psychophysics: Transforming numbers into movies. *Spatial Vision*, *10*(4), 437–442.

Rabagliati, H., Robertson, A., & Carmel, D. (2018). The importance of awareness for understanding language. *Journal of Experimental Psychology: General*, *147*(2), 190–208, https://doi.org/10.1037/xge0000348.

Ramamurthy, M., & Blaser, E. (2018). Assessing the kaleidoscope of monocular deprivation effects. *Journal of Vision*, *18*(13):14, 1–16, https://doi.org/10.1167/18.13.14. [PubMed] [Article]

Roseboom, W., & Arnold, D. H. (2011). Learning to reach for "invisible" visual input. *Current Biology*, *21*(13), R493–R494, https://doi.org/10.1016/j.cub.2011.05.036.

Rothkirch, M., & Hesselmann, G. (2018). No evidence for dorsal-stream-based priming under continuous flash suppression. *Consciousness & Cognition*, *64*, 84–94, https://doi.org/10.1016/j.concog.2018.05.011.

Rouder, J. N. (2014). Optional stopping: No problem for Bayesians. *Psychonomic Bulletin & Review*, *21*(2), 301–308, https://doi.org/10.3758/s13423-014-0595-4.

Rousselet, G. A., Pernet, C. R., & Wilcox, R. R. (2017). Beyond differences in means: Robust graphical methods to compare two groups in neuroscience. *European Journal of Neuroscience*, *46*(2), 1738–1748, https://doi.org/10.1111/ejn.13610.

Sakuraba, S., Sakai, S., Yamanaka, M., Yokosawa, K., & Hirayama, K. (2012). Does the human dorsal stream really process a category for tools? *Journal of Neuroscience*, *32*(11), 3949–3953, https://doi.org/10.1523/JNEUROSCI.3973-11.2012.

Schönbrodt, F. D., Wagenmakers, E. J., Zehetleitner, M., & Perugini, M. (2017). Sequential hypothesis testing with Bayes factors: Efficiently testing mean differences. *Psychological Methods*, *22*(2), 322–339, https://doi.org/10.1037/met0000061.

Schyns, P. G., & Oliva, A. (1994). From blobs to boundary edges: Evidence for time- and spatial-scale-dependent scene recognition. *Psychological Science*, *5*(4), 195–200, https://doi.org/10.1111/j.1467-9280.1994.tb00500.x.

Schyns, P. G., & Oliva, A. (1997). Flexible, diagnosticity-driven, rather than fixed, perceptually determined scale selection in scene and face recognition. *Perception*, *26*, 1027–1038, https://doi.org/10.1068/p261027.

Stein, T., & Sterzer, P. (2011). High-level face shape adaptation depends on visual awareness: Evidence from continuous flash suppression. *Journal of Vision*, *11*(8):5, 1–14, https://doi.org/10.1167/11.8.5. [PubMed] [Article]

Stein, T., Sterzer, P., & Peelen, M. V. (2012). Privileged detection of conspecifics: Evidence from inversion effects during continuous flash suppression. *Cognition*, *125*(1), 64–79, https://doi.org/10.1016/j.cognition.2012.06.005.

Sterzer, P., Haynes, J. D., & Rees, G. (2008). Fine-scale activity patterns in high-level visual areas encode the category of invisible objects. *Journal of Vision*, *8*(15):10, 1–12, https://doi.org/10.1167/8.15.10. [PubMed] [Article]

Sterzer, P., Stein, T., Ludwig, K., Rothkirch, M., & Hesselmann, G. (2014). Neural processing of visual information under interocular suppression: A critical review. *Frontiers in Psychology*, *5*: 453, https://doi.org/10.3389/fpsyg.2014.00453.

Sweeny, T. D., Grabowecky, M., & Suzuki, S. (2011). Awareness becomes necessary between adaptive pattern coding of open and closed curvatures. *Psychological Science*, *22*(7), 943–950, https://doi.org/10.1177/0956797611413292.

Tong, F., Nakayama, K., Vaughan, J. T., & Kanwisher, N. (1998). Binocular rivalry and visual awareness in human extrastriate cortex. *Neuron*, *21*(4), 753–759, https://doi.org/10.1016/S0896-6273(00)80592-9.

Tsuchiya, N., & Koch, C. (2005). Continuous flash suppression reduces negative afterimages. *Nature Neuroscience*, *8*, 1096–1101, https://doi.org/10.1038/nn1500.

Van Opstal, F., De Loof, E., Verguts, T., & Cleeremans, A. (2016). Spontaneous eyeblinks during breaking continuous flash suppression are associated with increased detection times. *Journal of Vision*, *16*(14):21, 1–10, https://doi.org/10.1167/16.14.21. [PubMed] [Article]

Yamins, D. L. K., & DiCarlo, J. J. (2016). Using goal-driven deep learning models to understand sensory cortex. *Nature Neuroscience*, *19*(3), 356–365, https://doi.org/10.1038/nn.4244.

Yang, E., & Blake, R. (2012). Deconstructing continuous flash suppression. *Journal of Vision*, *12*(3):8, 1–14, https://doi.org/10.1167/12.3.8. [PubMed] [Article]

Yang, E., Brascamp, J., Kang, M. S., & Blake, R. (2014). On the use of continuous flash suppression for the study of visual processing outside of awareness. *Frontiers in Psychology*, *5*: 724, https://doi.org/10.3389/fpsyg.2014.00724.

Yang, E., Zald, D. H., & Blake, R. (2007). Fearful expressions gain preferential access to awareness during continuous flash suppression. *Emotion*, *7*(4), 882–886, https://doi.org/10.1037/1528-3542.7.4.882.

Yu, K., & Blake, R. (1992). Do recognizable figures enjoy an advantage in binocular rivalry? *Journal of Experimental Psychology: Human Perception & Performance*, *18*(4), 1158–1173, https://doi.org/10.1037/0096-1523.18.4.1158.

Zabelina, D. L., Guzman-Martinez, E., Ortega, L., Grabowecky, M., Suzuki, S., & Beeman, M. (2013). Suppressed semantic information accelerates analytic problem solving. *Psychonomic Bulletin & Review*, *20*(3), 581–585, https://doi.org/10.3758/s13423-012-0364-1.